energies

Article

Distribution Strategy Optimization of Standalone Hybrid WT/PV System Based on Different Solar and Wind Resources for Rural Applications

Yan Yang [1,*], Qingyu Wei [2], Shanke Liu [3] and Liang Zhao [4]

1 School of Energy and Power Engineering, University of Shanghai for Science and Technology, Shanghai 200093, China
2 Beijing Aerospace Propulsion Institute, Beijing 100191, China; wei.1203@stu.xjtu.edu.cn
3 College of Smart Energy, Shanghai Jiao Tong University, Shanghai 200240, China; liushanke@sjtu.edu.cn
4 State Key Laboratory of Multiphase Flow in Power Engineering, Xi'an Jiaotong University, Xi'an 710049, China; lzhao@xjtu.edu.cn
* Correspondence: yyan@usst.edu.cn

Abstract: The characteristics of solar and wind energy determine that the optimization of a standalone hybrid wind turbine (WT)/photovoltaic panel (PV) system depends on the natural resources of the installation location. In order to ensure system reliability and improve the resource utilization, a method for determining the installed capacity ratio of a hybrid renewable energy system is required. This study proposes a calculation method to optimize the installed capacity ratio, considering the system reliability to meet the needs of the hybrid system to adapt to different natural resources. In this paper, a standalone hybrid WT/PV system to provide electricity for rural areas is designed. Taking the power supply guarantee rate and electricity supply continuity as indicators, the system is simulated by using the Transient System Simulator solver. The results show that the recommended installed capacity ratio of the WT and PV is 5:1 when the total solar irradiation is less than 5040 MJ/(m^2·a) and the annual average wind velocity is in the range of 3.0~3.5 m/s. When the annual average wind velocity is in the range of 2.0~3.0 m/s, the PV plays an increasingly significant role in the hybrid system and exceeds the WT if the total solar irradiation is greater than 6300 MJ/(m^2·a). However, if the total solar irradiation and the annual average wind velocity are less than 5040 MJ/(m^2·a) and 2.0 m/s, respectively, it is not recommended to use the standalone hybrid system because it cannot meet the power demand. These conclusions provide guidance for the distribution strategies of the standalone hybrid WT/PV system within different natural resources.

Keywords: hybrid system; distribution strategy; installed capacity ratio; solar and wind resources

Citation: Yang, Y.; Wei, Q.; Liu, S.; Zhao, L. Distribution Strategy Optimization of Standalone Hybrid WT/PV System Based on Different Solar and Wind Resources for Rural Applications. *Energies* **2022**, *15*, 5307. https://doi.org/10.3390/en15145307

Academic Editor: Branislav Hredzak

Received: 11 June 2022
Accepted: 19 July 2022
Published: 21 July 2022

1. Introduction

Renewable resources have attracted more and more attention due to the continuous energy demand and the impact of fossil fuels on the environment. Among all the renewable technologies, the photovoltaic panel (PV) and wind turbine (WT) are the most profitable ones [1]. However, the common disadvantage of wind and solar energy is their intermittency [2]. Both solar and wind resources are susceptible to weather fluctuations [3]. PV power generation in summer is usually higher than that in winter, while WT power generation increases during the winter seasons [4]. Therefore, taking advantage of the complementarity of these two resources and combining them properly to form a hybrid system can partially overcome the unpredictability [5]. In addition, because of a more stable overall annual power production, the hybrid system is extremely attractive [6], especially for remote areas [7]. Nevertheless, in the hybrid system, the power generation will inevitably fluctuate due to the oscillations of solar radiation and wind velocity. Hence, suitable battery banks are needed to mitigate the fluctuation of PV and WT power generation [8].

Li et al. carried out three standalone renewable energy systems for a household in Urumqi. The results showed that the hybrid WT/PV/battery power system is more suitable than the PV/battery and WT/battery power systems [9]. To calculate the optimum configuration of a hybrid WT/PV system, Yang et al. recommended an optimal design model employing battery banks [10,11]. The optimization variables of the model included the number and slope angle of the PV, the number and installation height of the WT, and the battery capacity. Ekren et al. optimized the hybrid WT/PV power system by a response surface methodology with the PV area, the swept area of the WT rotor, and the battery capacity as optimization variables [12]. Dihrab et al. simulated a hybrid system for grid-connected applications in three cities in Iraq using the MATLAB solver. The results showed that it is possible for Iraq to use solar and wind energy to generate power for some villages in the desert or rural areas [13]. Shivam et al. conducted the multiobjective optimization of solar wind hybrid systems at four different locations in southern Taiwan [14]. The simulation results showed that the photovoltaic modules were economical choices for the grid-connected mode, while the solar–wind hybrid systems were more environmentally friendly.

At present, there are many software tools that can be used for the design, analysis, and optimization of a hybrid renewable energy system, such as the Hybrid Optimization Model for Electric Renewables (HOMER), RETSCREEN, Transient System Simulator (TRNSYS), and so on. Al-Karaghouliand and Kazmerski proposed a photovoltaic solar system to power a health clinic in southern Iraq and estimated the system size and its life-cycle cost by HOMER [15]. A prefeasibility study of using hybrid energy systems with hydrogen as an energy carrier for applications was discussed by Khan and Iqbal [16]. Through the analysis and comparison using HOMER, it was found that the wind–diesel battery hybrid system had excellent potential. Zandi et al. conducted the economic analysis and the environmental impact of the photovoltaic system utilization in a residential sector using RETSCREEN [17]. The techno-economic and environmental sustainability of a grid-connected solar photovoltaic system was validated by Owolabi et al. [18]. According to the calculation results of RETSCREEN, the site selection of the solar photovoltaic project was recommended. Bakic et al. analyzed a hybrid WT/PV power system of Belgrade using the dynamical simulation method based on TRNSYS [19]. They predicted that the hybrid system could meet the annual electricity consumption by increasing the battery for energy storage. Panayiotou et al. analyzed the applications of a standalone PV system and standalone hybrid WT/PV system in two different locations by TRNSYS. They pointed out that the type of system directly depended on the climatic characteristics of the specific location [20]. Zappa and Broek found that the optimum capacity mix was 74% WT and 26% PV for the hybrid power system in Europe, which could satisfy 82% of the annual electricity demand [21], while the optimal distribution strategy was 5 WTs and 165 PVs for the hybrid power system in Korea, namely 10% WT and 90% PV, which supplied power to a wastewater treatment plant [22]. However, HOMER does not consider the battery bank depth of discharge, a key factor affecting the life and size of the battery bank, in hybrid system optimization. Moreover, RETSCREEN does not take into account the effect of temperature for PV performance analysis [23]. The main feature of TRNSYS is that it can flexibly modify the model, control strategy, and system configuration [24]. In a comprehensive consideration, TRNSYS is a good choice for analyzing and optimizing the performance of hybrid systems.

There are two reasons for the different optimal configuration of the hybrid system: one is the difference of the solar and wind resources, and the other is the difference of the load. Therefore, for the hybrid WT/PV system, the biggest challenge is not the variability or intermittency of solar and wind resources, but how to combine the load and these resources to formulate an optimal distribution strategy, and then develop a suitable system design solution. In this way, the solar and wind resources can be fully utilized, and the power availability and system efficiency can be improved. However, most of the existing studies focus on the optimization of the hybrid WT/PV system in a certain region but lack the classification discussion and system optimization design based on different solar and wind resources.

In the past decade, China's consumption of renewable energy has been increasing, and renewable energy has replaced nonrenewable energy more and more [25]. China has set ambitious targets to control carbon emissions by 2030 or earlier and intends to increase the use ratio of low-carbon energy to 20% [26]. This will lead to more renewable energy being incorporated into the Chinese power system, especially wind and solar energy. According to the latest China 2050 High Renewable Energy Penetration Scenario and Roadmap Study from the Energy Research Institute National Development and Reform Commission of China, the installed capacities of WTs and PVs will reach 64% of Chinese total power generation by 2050 [27]. However, there are still some problems in China's renewable energy development. Particularly, the distributions of solar and wind resources are uneven. This will lead to regional heterogeneity of renewable energy utilization. Many studies have conducted initial assessments of solar and wind resources within China as a necessary precursor to their utilization [28–32].

In this paper, a standalone hybrid WT/PV system is designed for rural electricity consumption as the load, and the optimal distribution strategies suitable for different regions are proposed by taking the different solar and wind resources in 26 regions of China. It is hoped that the research results of this paper could provide systematic design ideas and distribution strategies for areas with similar natural resources.

2. Theory and Methodology

2.1. System Description

In this study, the software used for the modeling and simulation is TRNSYS. The standalone hybrid WT/PV system is established as shown in Figure 1.

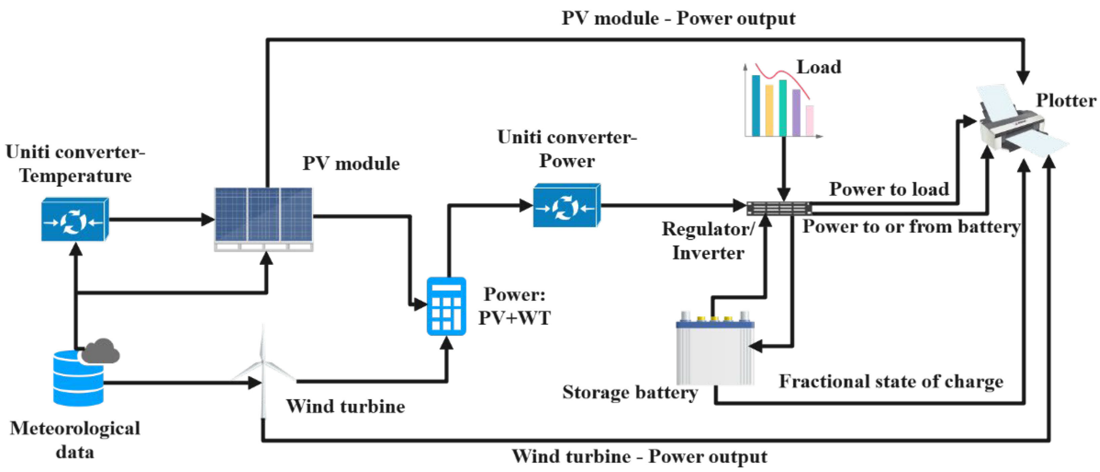

Figure 1. Model of standalone hybrid WT/PV system by TRNSYS.

The main components used in the model of the standalone hybrid WT/PV system are:

(1) PV module. TRNSYS Type 94 models the electrical performance of a photovoltaic array. In this type, the current–voltage characteristics of a single module are predicted by an empirical equivalent circuit model.
(2) Wind turbine. TRNSYS Type 90 models a wind turbine. It makes use of some readily available manufacturer data as well as analytical solutions. In this type, the energy extracted by a wind turbine results from the change in momentum of the air moving through the rotor.
(3) Storage battery. TRNSYS Type 47 operates in conjunction with solar cell array and power conditioning components. In this type, the battery state of charge varies over time and can be obtained given the rate of charge or discharge.

(4) Regulator and inverter. TRNSYS Type 48 models both the regulator and inverter. In this type, the regulator distributes the power from the PV and WT to and from the battery, and the inverter converts the DC power to AC and sends it to the load.

The mathematical descriptions of above types are shown in Section 2.2. The strength of the current source by the PV module and the power produced by the wind turbine are simulated based on the manufacturer data, empirical formulas, and the natural resources.

2.2. System Components

2.2.1. PV Module

To simulate the PV module, the "five-parameter" equivalent circuit model included in Type 94 is used. The five parameters included in the model are: (1) $I_{L,ref}$, module photocurrent at reference condition; (2) $I_{O,ref}$, diode reverse saturation current at reference condition; (3) γ, empirical PV curve-fitting parameter; (4) R_s, module series resistance; (5) R_{sh}, module shunt resistance.

The current–voltage equation for the equivalent circuit is [33]:

$$I = I_L - I_o\left\{\exp\left[\frac{q}{\gamma k T_c}(V + IR_s)\right] - 1\right\} - \frac{V + IR_s}{R_{sh}} \tag{1}$$

where I_L is the module photocurrent, I_O is diode reverse saturation current, q is electron charge constant, k is Boltzmann constant, and T_c is module temperature.

The negative reciprocal of the short-circuit IV slope closely approximates the shunt resistance:

$$R_{sh} \approx \frac{-1}{(dI/dV)_{V=0}}. \tag{2}$$

Equation (2) reduces the number of unknown quantities to four. Rearranging Equation (1) at open-circuit, short-circuit, and maximum power conditions yields, $I_{L,ref}$, $I_{O,ref}$, γ, which can be written as the following expressions:

$$I_{L,ref} = I_{SC,ref}\left(1 + \frac{R_s}{R_{sh}}\right) \tag{3}$$

$$I_{o,ref} = \frac{I_{L,ref} - V_{OC,ref}/R_{sh}}{\exp\left(\frac{q}{\gamma k T_{c,ref}} V_{OC,ref}\right)} \tag{4}$$

$$\gamma = \frac{q\left(V_{mp,ref} - V_{OC,ref} + I_{mp,ref}R_s\right)}{kT_{c,ref}\ln\left(\frac{I_{L,ref} - I_{mp,ref} - \frac{V_{mp,ref} + I_{mp,ref}R_s}{R_{sh}}}{I_{SC,ref}V_{OC,ref}/R_{sh}}\right)} \tag{5}$$

where $I_{SC,ref}$ is the short-circuit current at reference condition, $V_{OC,ref}$ is the open-circuit voltage at reference condition, $T_{c,ref}$ is module temperature at reference condition, $V_{mp,ref}$ is the voltage at maximum power point along IV curve with reference condition, and $I_{mp,ref}$ is current at maximum power point along IV curve with reference condition.

For the sake of finding the correct values for R_s and γ, an iterative search routine is used by matching the analytical value for the temperature coefficient of the open-circuit voltage. The last equation is derived from the analytical derivative of voltage to temperature under the reference open-circuit condition.

$$\frac{\partial V_{OC}}{\partial T_c} = \mu_{Voc} = \frac{\mu_{Isc} - I_{o,ref}\left(3 + \frac{q\varepsilon}{AkT}\right)\exp\left(\frac{q}{k\lambda T_{c,ref}}\right)/T_c}{\frac{q}{k\lambda T_{c,ref}} I_{o,ref}\exp\left(\frac{q}{k\lambda T_{c,ref}} V_{OC,ref}\right) + \frac{1}{R_{sh}}} \tag{6}$$

where μ_{Voc} is the temperature coefficient of open-circuit voltage, μ_{Isc} is the temperature coefficient of short-circuit current, ε is semiconductor bandgap, and A is the ratio of γ to individual cells number in the module.

To compute the module temperature at each timestep, the temperature data from standard nominal operating cell temperature (NOCT) measurements are used. The module loss coefficient is determined by the NOCT data.

$$\frac{\tau\alpha}{U_L} = \frac{T_{c,NOCT} - T_{a,NOCT}}{G_{T,NOCT}} \tag{7}$$

where $\tau\alpha$ is module transmittance–absorptance product, U_L is module loss coefficient, $T_{c,NOCT}$ is module temperature at NOCT conditions, $T_{a,NOCT}$ is ambient temperature at NOCT conditions, and $G_{T,NOCT}$ is incident radiation at NOCT conditions.

The module temperature at any timestep can be written as follows, assuming that the ratio of the module transmittance–absorptance product to the module loss coefficient is constant:

$$T_c = T_a + \frac{1 - \frac{\eta_c}{\tau\alpha}}{\frac{G_T \tau\alpha}{U_L}} \tag{8}$$

where η_c is the conversion efficiency of the module, which varies with ambient conditions.

YL-280-30b is selected in this study, and the technical data is shown in Table 1. The PV modules are placed horizontally towards the south.

Table 1. Technical data of PV module.

Parameters	Value
Module short-circuit current at reference condition	9.61 A
Module open-circuit voltage at reference condition	38.90 V
Reference temperature	298.00 K
Reference insolation	1000.00 W·m^{-2}
Module voltage at max. power point and reference condition	31.10 V
Module current at max. power point and reference condition	9.01 A
Temperature coefficient of I_{sc} at reference condition	0.04%/K
Temperature coefficient of V_{oc} at reference condition	−0.31%/K
Number of cells wired in series	60
Module temperature at NOCT	319.00 K
Ambient temperature at NOCT	293.00 K
Insolation at NOCT	800.00 W·m^{-2}
Module area	1.46 m^2
Module transmittance–absorptance product	0.95
Semiconductor bandgap	1.12

2.2.2. Wind Turbine

To simulate the wind turbine, some readily available manufacturer data, as well as analytical solutions included in Type 90, are used. The impact of the air density and hub height is considered in turbine power output. Wind turbines transform the kinetic energy of moving air into useful work. The power output of a wind turbine can be written as:

$$P_{WT} = 0.5 C_p \rho A_{WT} U^3 \tag{9}$$

$$C_p = 4a(1-a)^2 \tag{10}$$

where C_p is the power coefficient as a function of the axial induction factor a, ρ is the air density, A_{WT} is area of the rotor, and U is wind velocity in the free stream.

The mass flow rate of air is a function of its density. Introducing the ideal gas law mboxemphp = ρRT, the pressure difference from one altitude to another can be written as:

$$\int_1^2 \frac{dp}{p} = \ln\frac{p_2}{p_1} = -\frac{g}{R}\int_1^2 \frac{dz}{T}. \tag{11}$$

For elevations where wind energy applications apply, temperature decreases linearly with altitude [34]:

$$T(z) \approx T_o - Bz \tag{12}$$

where B = 6.5 K/km of altitude.

Then an expression for pressure decrease with altitude can be obtained taking into account the temperature lapse rate:

$$p_2 = p_1\left(1 - \frac{Bz}{T_o}\right)^{\frac{g}{RB}} \tag{13}$$

where T = 288 K.

The modeling of wind velocity per change in height above the ground is based on the boundary layer theory of atmosphere [35]:

$$\frac{U_1}{U_2} = \left(\frac{z_1}{z_2}\right)^{\alpha} \tag{14}$$

where α determines the rate of wind velocity increase as a function of height. Under ideal boundary layer conditions, the value of α is taken to be 1/7.

Three kinds of wind turbines are selected to adapt to different distribution strategies of the hybrid system. The technical data of them are shown in Table 2. The power output curves from the manufacturer are used, as shown in Figure 2. These data are gleaned from Guangzhou Infinite Wind Power Generator Manufacture Co., Ltd.

Table 2. Technical data * of wind turbines.

Type	Parameters	Value
MAX-1600W	Rated power	1.60 kW
	Cut-in wind speed	2.50 m·s^{-1}
	Rated wind speed	12.00 m·s^{-1}
	Diameter of blade	2.20 m
	Hub height	8.00 m
MAX-800W	Rated power	0.80 kW
	Cut-in wind speed	2.00 m·s^{-1}
	Rated wind speed	12.00 m·s^{-1}
	Diameter of blade	1.80 m
	Hub height	8.00 m
MINI-400W	Rated power	0.40 kW
	Cut-in wind speed	2.00 m·s^{-1}
	Rated wind speed	12.00 m·s^{-1}
	Diameter of blade	1.16 m
	Hub height	8.00 m

* Data Sources: [36].

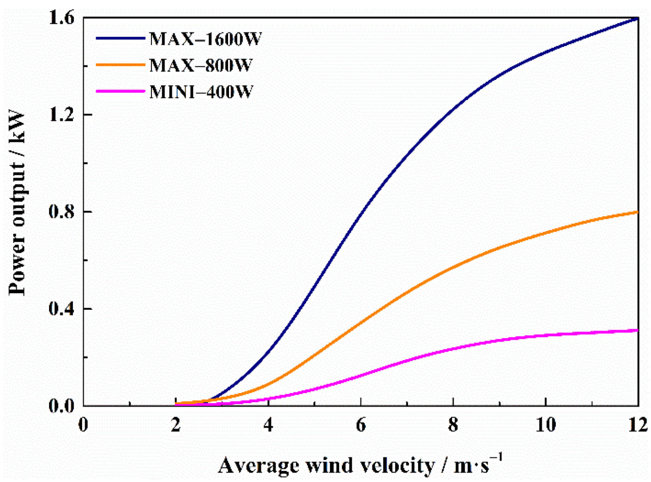

Figure 2. Power output curves of wind turbines.

2.2.3. Storage Battery

Currently, lithium-ion and lead–acid are the commonly used batteries in stationary applications [37]. Among them, lead–acid battery is a popular choice for storing uninterruptible power supply due to its low cost, reliability, and efficiency [38]. The university of Navarra had built a microgrid platform that used a lead–acid battery pack consisting of 120 FIAMM SMG300 cells in series as its storage component [39]. A stand-alone hybrid power generation for a remote community in Bangladesh was studied by Das et al. [40]. Due to the participation of lead–acid batteries, the system could satisfy the energy demand of a primary load of 248 kWh/day and a peak load of 44.41 kW. Therefore, this paper chooses the lead–acid battery as the power storage component of the system. To simulate the lead–acid storage battery, the Hyman model which is more realistic at very low currents included in Type 47 is used.

On discharge, the formula is:

$$V = V_{oc} - V_{zp} - g_d H + I r_{qd}\left(1 + \frac{m_d H}{Q_d/Q_m - H}\right). \tag{15}$$

On charge, it is:

$$V = V_{oc} - V_{zp} - g_c H + I r_{qc}\left(1 + \frac{m_c H}{Q_c/Q_m - H}\right) \tag{16}$$

where

$$H = 1 - FSOC = 1 - \frac{Q}{Q_m} \tag{17}$$

V_{oc} is the open circuit voltage at full charge, V_{zp} is an additional voltage term in Hyman model, g_c and g_d are small-valued coefficients of H in voltage–current state, FSOC is the fractional state of the charge, Q is the state of the charge, Q_m is rated capacity of the cell, r_{qc} and r_{qd} are internal resistances, m_c and m_d are cell-type parameters which determine the shapes of the I-V-Q characteristics, and Q_c and Q_d are capacity parameters on the charge and discharge.

To prolong the battery life, the battery should not be charged to too high a voltage or discharged to too low a voltage. The cutoff voltage on charge (V_c) and discharge (V_d) will be used in the regulator and inverter module so that the voltage charging and discharging can be initiated so to ensure not to exceed V_c or to drop below V_d.

Sail-GFM-200 is selected as the storage battery and the technical data are shown in Table 3.

Table 3. Technical data of storage battery.

Parameters	Value
Cell energy capacity	200.00 Ah
Charging efficiency	0.90
Max. current per cell charging	37.70 A
Max. current per cell discharging	−37.70 A
Rated voltage	2.00 V
Max. charge voltage per cell	2.35 V
Calculate discharge cutoff voltage	1.60 A

Taking into account the complementarity of solar and wind energy in terms of time, the number of self-contained days for the battery is selected as one day in the system design. Then, the total energy capacity of the battery is:

$$B_c = \frac{N_0 Q_L}{\eta D} \tag{18}$$

where N_0 is the number of self-contained days, Q_L is the daily average of annual electricity consumption, η is the inverter efficiency, and D is the maximum discharge depth.

The number of batteries in series:

$$N_s = \frac{V}{V_0} \tag{19}$$

where V is the input voltage of the inverter and V_0 is the rated voltage of the battery.

The number of batteries in parallel:

$$N_p = \frac{B_c}{A_c V} \tag{20}$$

where A_c is the energy capacity of a single battery.

2.2.4. Regulator and Inverter

The battery's voltage level and charge/discharge rate as well as its state of charge will be monitored using Type 48. The charge to discharge limit on the fractional state of charge (F_B) is an important parameter in the regulator and inverter. If FSOC < F_B and the battery has been charging, then the battery must be on the "total charge" state. On the "total charge," the first priority is given to recharging the battery rather than sending the output to the load until FSOC > F_B. The technical data of the regulator and inverter are shown in Table 4.

Table 4. Technical data of regulator and inverter.

Parameters	Value
Regulator efficiency	0.90
Inverter efficiency, DC to AC	0.90
Inverter efficiency, AC to DC	0.90
High limit on FSOC	1.00
Low limit on FSOC	0.00
Charge to discharge limit on FSOC	0.30
Input voltage of inverter	24.00 V
Power output limit	1.00 kW

2.3. Load Characteristics

To determine the load profile over a specific period of time, Type 14 h is used. TRNSYS Type 14 h provides a time-dependent forcing function model in transient simulation. The pattern of the forcing function is established by a set of discrete data points indicating its values at various times through one cycle. The hourly electricity consumption of rural residences in China is used as the load data in this study [41], as shown in Figure 3. The referenced hourly electricity consumption is the statistical value of 30 rural residences' test results, which reflects the characteristics of rural residential electricity consumption in different months in China. The annual electricity consumption is divided into three stages, namely the transition stage, the heating stage, and the air conditioning stage. May, June, September, and October are the transition stage. January, February, March, April, November, and December are the heating stage. July and August are the air conditioning stage. It can be seen from the figure that the hourly electricity consumption of rural residences presents the characteristics of three waves, and the occurrence time of the wave in the morning has variation at different stages which is in line with the reality of life. It needs to be explained here that China's rural energy consumption structure is developing towards a clean type, but the heating mode in winter is mainly coal burning [42]. Therefore, the electricity consumption of heating in winter is not considered in this paper.

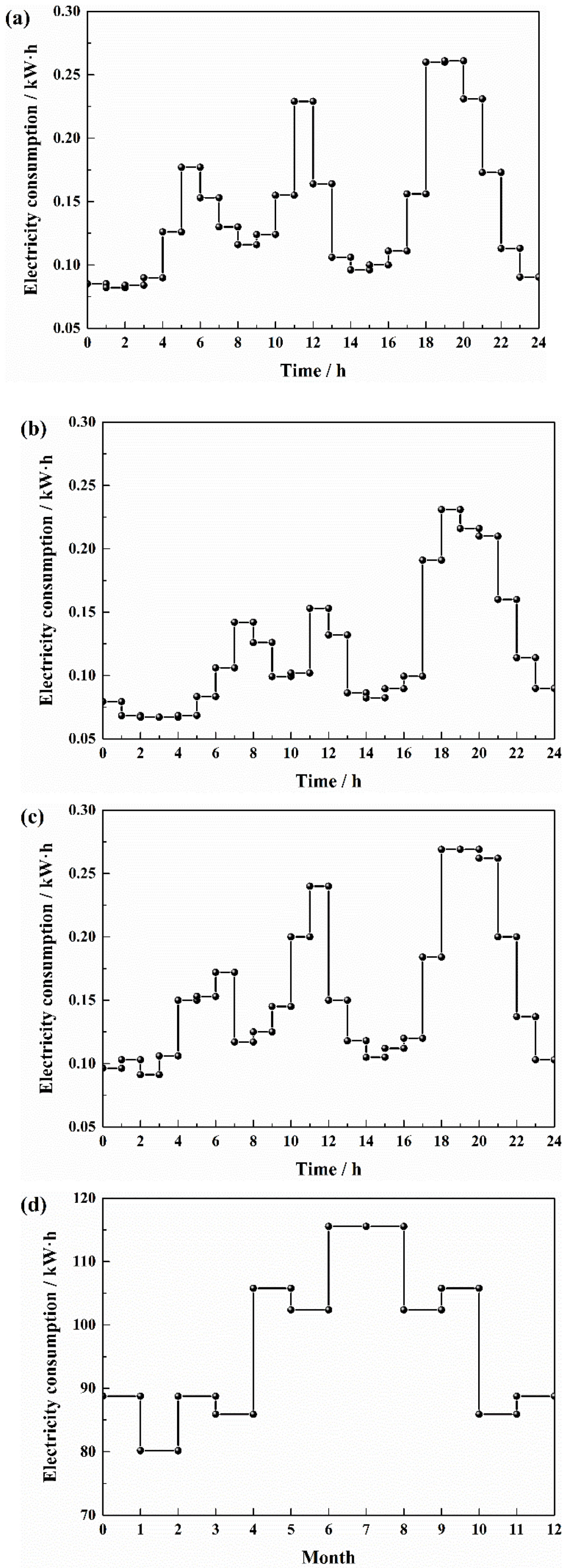

Figure 3. Electricity consumption: (**a**) Daily data of transition season; (**b**) Daily data of heating season; (**c**) Daily data of air conditioning season; (**d**) Monthly data.

2.4. Meteorological Data

For the sake of optimizing the distribution strategy of the hybrid system in different solar and wind resources, 26 regions of China are taken as samples, as shown in Figure 4.

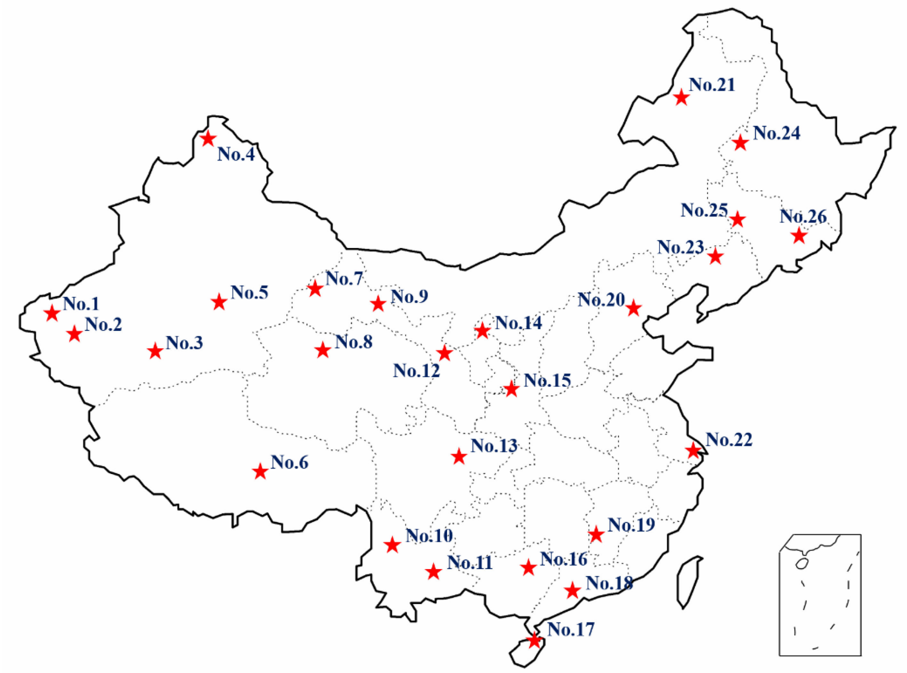

Figure 4. Geographic position of 26 regions in China.

According to the classification of solar energy resources (SER) in China [32], there are four categories based on the total solar irradiation: (I) greater than 6660 MJ/(m^2·a); (II) 6300~6660 MJ/(m^2·a); (III) 5040~6300 MJ/(m^2·a); (IV) less than 5040 MJ/(m^2·a). According to the classification of wind energy resources in China [31], there are six categories. However, the areas with the best and worst wind energy are small in China, so the wind energy resources (WER) in this study are classified into four categories based on the annual average wind velocity: (I) 3.0~3.5 m/s; (II) 2.5~3.0 m/s; (III) 2.0~2.5 m/s; (IV) less than 2.0 m/s.

The geographic conditions and natural resources classification of 26 regions in China are shown in Table 5. Hourly meteorological data are extracted from the TRNSYS database for a complete year.

Table 5. Geographic conditions and natural resources classification of 26 regions in China.

No.	Name	Geographic Position	Elevation	SER	WER
1	Kashi	37.83° N, 76.65° E	1289.0	II	III
2	Shache	38.42° N, 77.24° E	1231.0	II	IV
3	Andir	37.07° N, 82.68° E	1261.0	I	IV
4	Kaba-He	48.39° N, 86.34° E	1627.0	I	I
5	Tikanlik	39.02° N, 88.17° E	889.0	II	III
6	Lhasa	29.68° N, 91.02° E	3658.0	I	III
7	Dunhuang	40.14° N, 94.66° E	1139.0	II	II
8	Golmud	36.42° N, 94.90° E	2808.0	I	II
9	Jiuquan	39.44° N, 98.31° E	1480.0	II	II
10	Dali	25.60° N, 100.23° E	1990.5	III	III
11	Kunming	25.05° N, 102.72° E	1891.4	III	IV
12	Lanzhou	36.07° N, 103.82° E	1525.0	III	I
13	Chengdu	30.67° N, 104.07° E	505.9	IV	IV
14	Yinchuan	38.47° N, 106.28° E	1111.5	II	I

Table 5. *Cont.*

No.	Name	Geographic Position	Elevation	SER	WER
15	Xian	34.27° N, 108.93° E	396.9	III	III
16	Guilin	25.27° N, 110.30° E	150.0	IV	III
17	Haikou	20.03° N, 110.32° E	14.1	III	II
18	Guangzhou	23.13° N, 113.27° E	6.6	III	II
19	Ganzhou	25.83° N, 114.93° E	109.0	IV	IV
20	Beijing	39.90° N, 116.40° E	31.2	IV	II
21	Hailar	49.22° N, 119.77° E	617.0	II	I
22	Shanghai	31.23° N, 121.47° E	4.5	IV	I
23	Shenyang	41.80° N, 123.43° E	41.6	III	I
24	Qiqihar	47.35° N, 123.95° E	149.0	III	II
25	Siping	43.10° N, 124.22° E	164.2	IV	I
26	Yanji	42.93° N, 129.52° E	176.8	III	III

2.5. Distribution Strategy

Based on the electricity consumption in rural areas, the average generating capacity of the hybrid system is 3.12 kWh/day. Taking this value as the benchmark, the distribution strategies of total power with the different installed capacity ratios of the PV and WT are shown in Table 6.

Table 6. Distribution strategies of total power with the different installed capacity ratios of WT and PV.

Installed Capacity Ratio of WT and PV	5:1	3:1	2:1	1:1	1:2	1:3	1:5
Number of PV modules in series	1	1	1	1	1	1	1
Number of PV modules in parallel	2	3	4	6	8	9	10
Number of wind turbines—1.60 kW	1	1	1	1	0	0	0
Number of wind turbines—0.80 kW	1	1	0	0	1	1	0
Number of wind turbines—0.40 kW	1	0	1	0	1	0	2

Because the voltage at reference condition with a maximum power point of the PV module is 31.10 V and the input voltage of inverter is 24.00 V, the number of PV modules in the series is one. The number of PV modules in parallel can be calculated by:

$$N_{PV-p} = \frac{P_{PV}}{N_{PV-s}P_e} \tag{21}$$

where P_{PV} is the generating capacity of the PV modules, N_{PV-s} is the number of PV modules in series, and P_e is the maximum power at the reference condition.

2.6. Procedure of Methodology

The procedure of the methodology of this study is shown in Figure 5. Based on TRNSYS, through three types of input data, the power supply guarantee rate and electricity supply continuity under different distribution strategies are obtained. Then, the recommended installed capacity ratio of the region is proposed after comparing the results. After that, the distribution strategies suitable for different natural resources are summarized by the simulation of different regions.

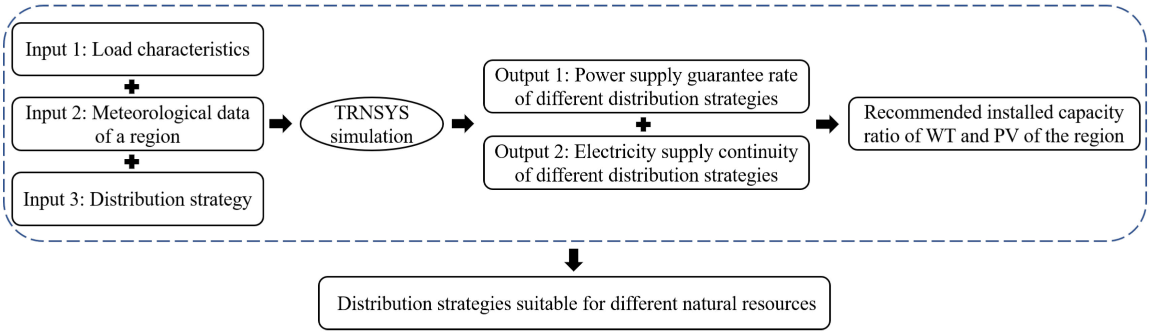

Figure 5. Flowchart for the methodology of this study.

3. Results and Discussion

3.1. Model Verification

To verify the modules utilized by TRNSYS in this paper, the meteorological data and the sizes of the PV and WT in the literature are used [13]. The solar irradiation and wind velocity distributions during the year are shown in Figure 6a according to the literature. The comparisons of the power output between the literature data and the simulated data of TRNSYS are shown in Figure 6b. The specifications of the PV module and the WT are shown in Table 7. It can be seen that the power output of the simulation results during the year are in good agreement with the literature data. The maximum relative error is only 7.15%, which verifies the model reliability of the PV module and the WT in TRNSYS.

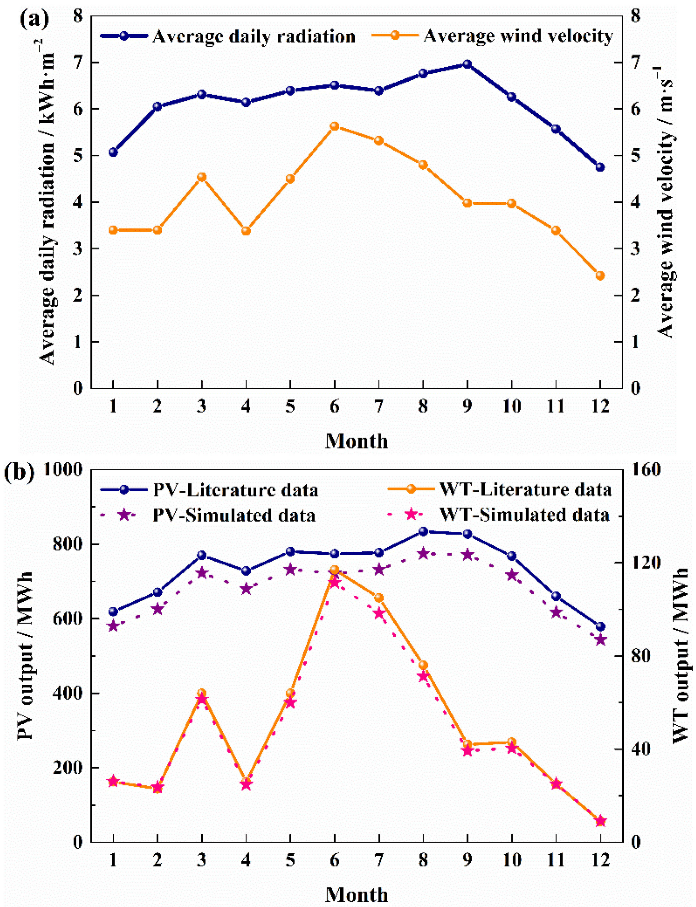

Figure 6. Model verification: (**a**) meteorological data; (**b**) result comparison.

Table 7. Specifications of PV module and WT in model verification.

Type	Specification	Value
PV module	Module open-circuit voltage at reference condition	21.70 V
	Module short-circuit current at reference condition	5.34 A
	Module voltage at max. power point and reference condition	17.40 V
	Module current at max. power point and reference condition	5.02 A
	Module area	0.66 m^2
	Temperature coefficient of I_{sc} at reference condition	0.002 A·K^{-1}
	Temperature coefficient of V_{oc} at reference condition	−0.082 V·K^{-1}
	Module temperature at NOCT	320.00 K
WT	Rated power	10.00 kW
	Rated wind speed	13.00 m·s^{-1}
	Diameter of blade	7.00 m

3.2. Case Analysis

In this section, two representative regions are selected to analyze the influence of the different distribution strategies on the hybrid system.

3.2.1. Case One

Wind and Solar Resources

Kaba-He is chosen for its abundance of solar and wind energy. Its wind and solar resources are both in the range of the first category. The daily radiation and wind velocity data of different months in a year are shown in Figure 7. As can be seen from the figure, solar energy and wind energy complement each other in a day. Solar radiation is intermittent, and its value is zero at night. However, although there is no fixed trend in wind velocity over the course of the day, the wind velocity is generally higher at night. The monthly average radiation and wind velocity data of Kaba-He are shown in Figure 8. It can be seen that solar energy and wind energy also complement each other over the months. The average solar radiation increases first and then decreases with the increase of month, whereas the trend of average wind velocity is opposite to that of average radiation.

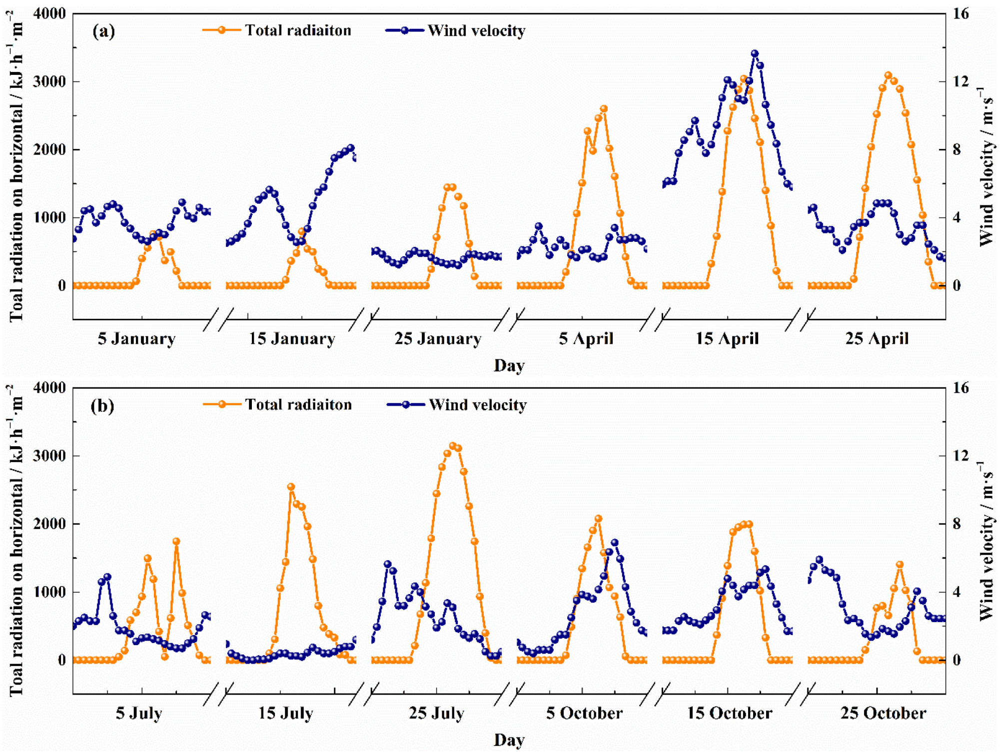

Figure 7. Daily radiation and wind velocity of different months in Kaba-He: (**a**) 5/15/25 January and 5/15/25 April; (**b**) 5/15/25 July and 5/15/25 October.

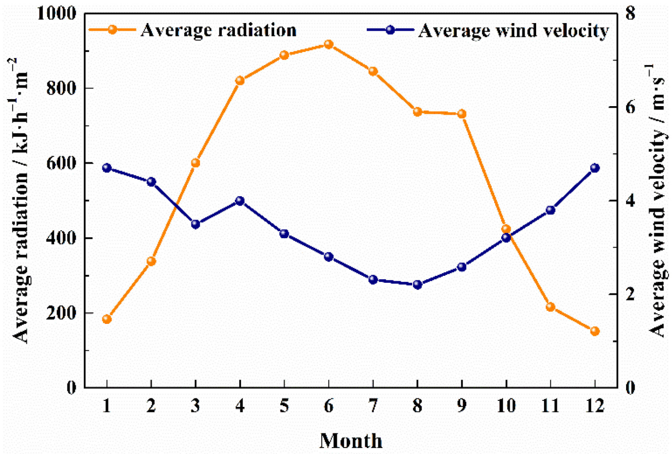

Figure 8. Monthly average radiation and wind velocity in Kaba-He.

Hourly Characteristics in Typical Days

When the installed capacity ratio of the WT and PV is 5:1, the hourly characteristics for two typical days (15 January and 15 July) are shown in Figure 9. Combined with the radiation and wind velocity data on January 15 (Figure 7), it can be seen that the power output of the WT and PV are consistent with the changes of the wind velocity and radiation. On 15 January 15, the maximum wind velocity is 8.10 m·s^{-1} at 23:00, and the WT output is 2188.01 W at the same time. The maximum radiation is 795.60 kJ·h^{-1}·m^{-2} at 14:00, and the PV output is 99.94 W at the same time. As shown in Figure 9b, the battery is in a state of neither charging nor discharging for two periods (9:00~11:00 and 17:00~24:00). This is because the FSOC value of the battery is greater than the upper limit of 1.00 during those periods, while the WT and PV output can meet the load consumption and there is excess power. The excess power will be dumped by the system, as shown in Figure 9a. On 15 July, the wind resource is poor, and the WT output is very little as the wind velocity is not up to the cut-in wind velocity. The load electricity consumption mainly comes from the battery and PV output. As shown in Figure 9d, before 11:00, the battery is in the discharge state, and the FSOC goes down from 0.97 to 0.95; between 12:00 and 16:00, the battery is in the charge state, and the FSOC goes up from 0.95 to 0.96; after 17:00, the battery is in the discharge state. It can be seen from Figure 9c that from 8:00 to 22:00, the PV output is greater than zero, while the PV output could only not meet the load electricity consumption from 12:00 to 16:00, and there is a surplus which will be stored in the battery.

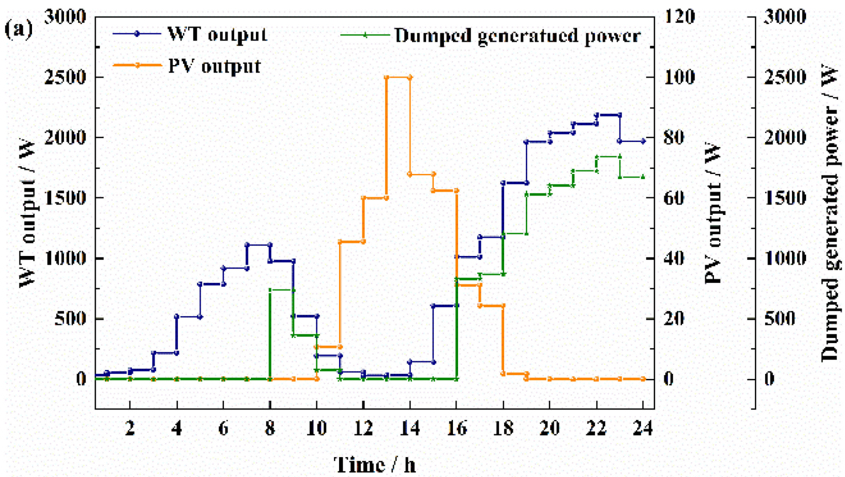

Figure 9. *Cont.*

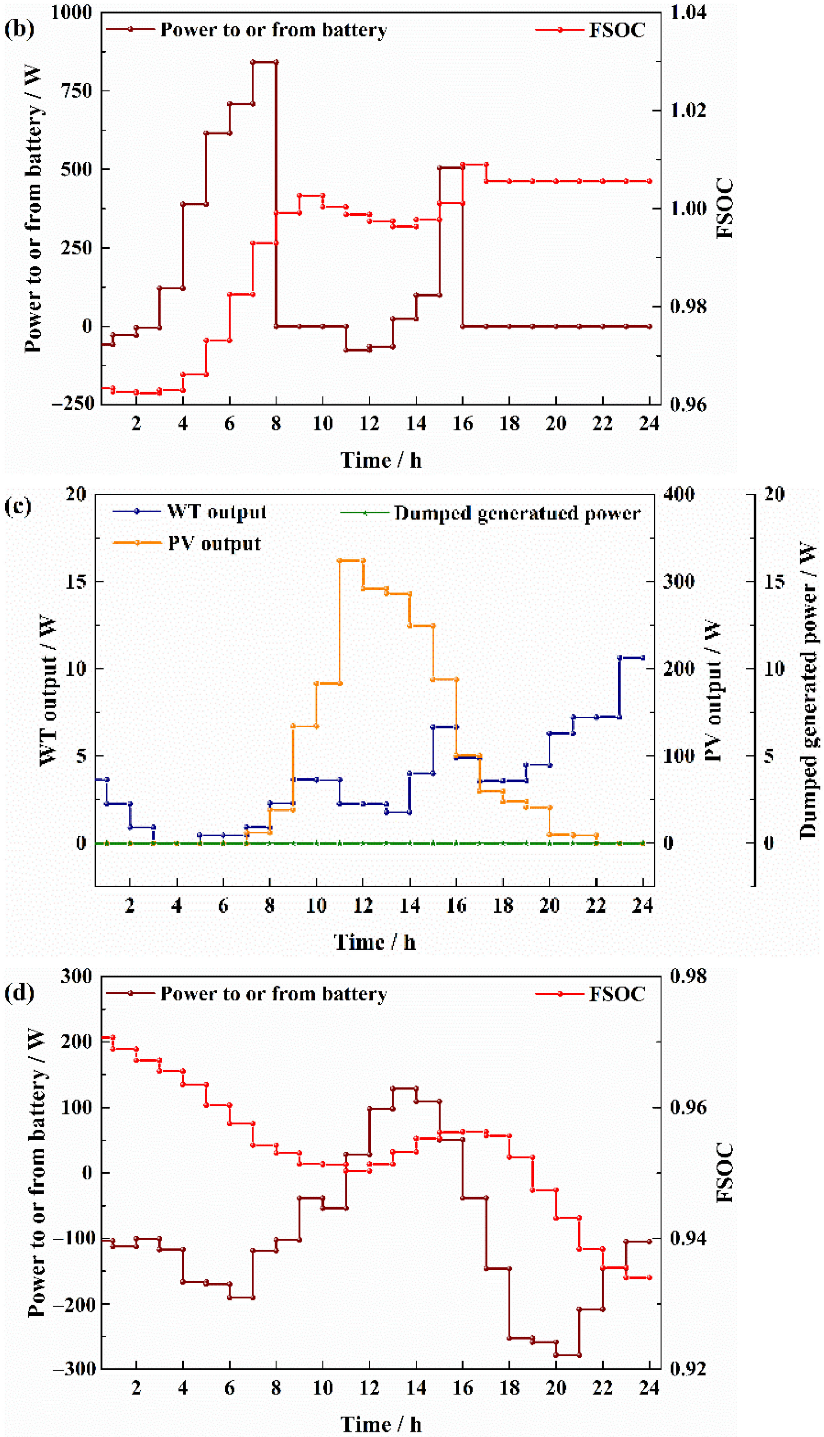

Figure 9. Hourly characteristics when the installed capacity ratio of WT and PV is 5:1 in Kaba-He: (**a**,**b**) for 15 January; (**c**,**d**) for 15 July.

Effect of Different Distribution Strategies

To compare the influence of different distribution strategies on the hybrid system, the power supply guarantee rate is used as an evaluation index. The power supply guarantee rate with the different installed capacity ratios of the WT and PV are shown in Figure 10. The power supply guarantee rate does not reach 100% because the battery is in a state of no power at first. The WT and PV output obtained in the early stage need to be charged to the battery until the FSOC reaches the threshold (0.30). The hourly FSOC of the first ten days and the start time of the electricity supply continuity with the different installed capacity ratios of the WT and PV are shown in Figure 11. As shown in Figure 10, the power supply guarantee rate varies little when the installed capacity ratios of the WT and PV are 5:1~1:1. When the ratio is less than 1:1, the power supply guarantee rate decreases obviously. This is because when the ratio is from 5:1 to 1:1, it takes around 5 days for the FSOC to become greater than 0.30. In addition, the system can guarantee the continuity of the electricity supply when the FSOC is greater than 0.30. However, when the ratio is less than 1:1, as an example of 1:2, although the FSOC reaches 0.30 at 136 h, it fluctuates between 0.28 and 0.31 until 191 h, so the start time of the electricity supply continuity is 191 h. Therefore, according to the wind and solar resources of Kaba-He, the recommended installed capacity ratios of the WT and PV for the hybrid system is from 5:1 to 1:1.

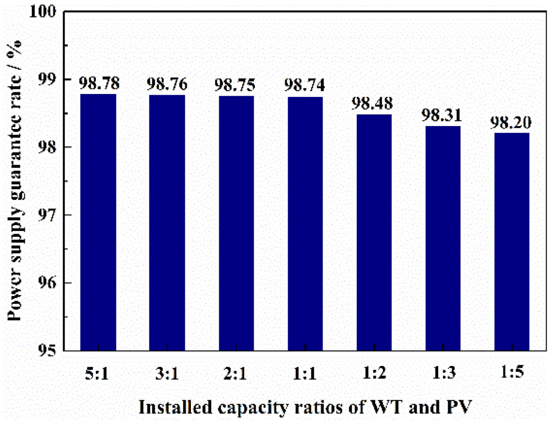

Figure 10. Power supply guarantee rate with different installed capacity ratios of WT and PV in Kaba-He.

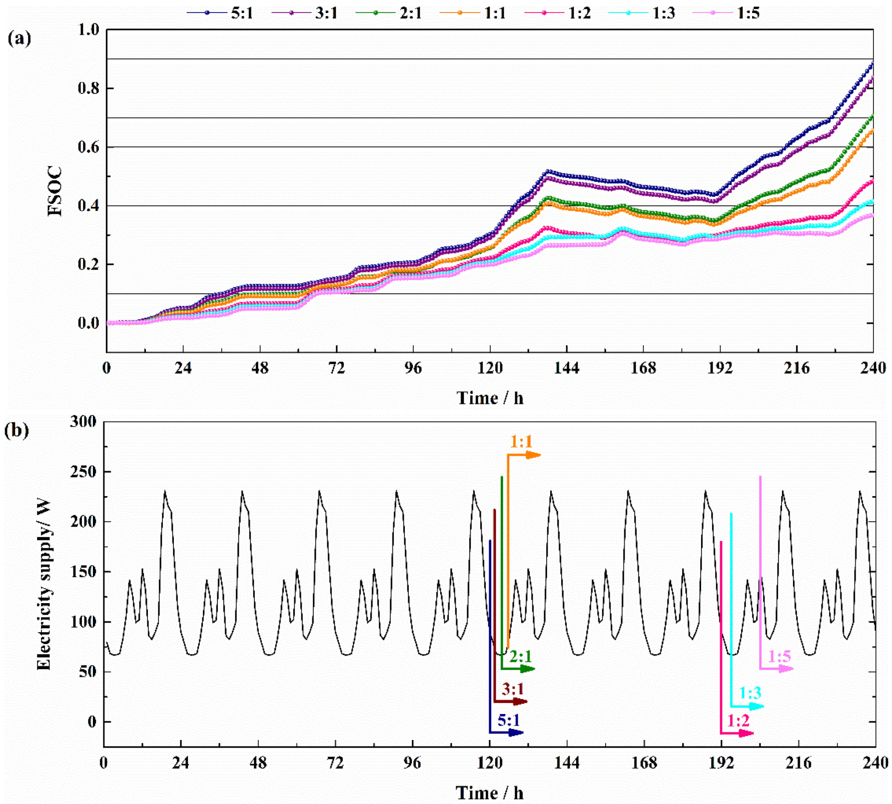

Figure 11. Hourly characteristics of the hybrid system in Kaba-He: (**a**) FSOC of the first ten days; (**b**) the start time of electricity supply continuity with different installed capacity ratios of WT and PV.

3.2.2. Case Two

Andir is chosen because it is rich in solar energy but short on wind energy. Its solar energy resource is in the range of the first category, whereas the wind energy resource is in the range of the fourth category. The monthly average radiation and wind velocity in Andir are shown in Figure 12. It can be seen that the maximum average wind velocity is 1.82 m·s^{-1} in March and the minimum average wind velocity is 0.90 m·s^{-1} in December.

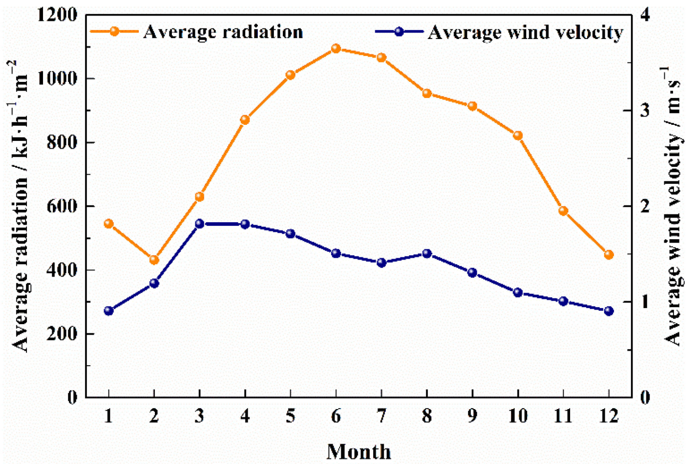

Figure 12. Monthly average radiation and wind velocity in Andir.

The power supply guarantee rate with the different installed capacity ratios of the WT and PV in Andir are shown in Figure 13. The hourly FSOC of the first twenty days and the start time of the electricity supply continuity are shown in Figure 14. As shown in Figure 13, the power supply guarantee rate rises significantly when the installed capacity ratio of the WT and PV is from 5:1 to 1:1. When the ratio is less than 1:1, the power supply guarantee rate increases slowly. This is because when the ratio is greater than 1:1, as an example of 2:1, although the FSOC reaches 0.30 at 184 h, it fluctuates between 0.28 and 0.31 until 469 h, so the start time of electricity supply continuity is 469 h. However, when the ratio is less than 1:1, as an example of 1:5, it takes 86 h for the FSOC to become greater than 0.30, and the system can guarantee the continuity of the electricity supply after that time. Therefore, according to the wind and solar energy resources of Andir, the recommended installed capacity ratio of the WT and PV of the hybrid system is 1:5.

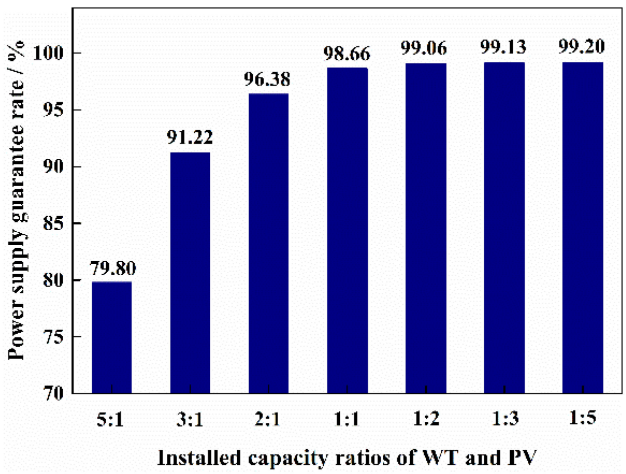

Figure 13. Power supply guarantee rate with different installed capacity ratios of WT and PV in Andir.

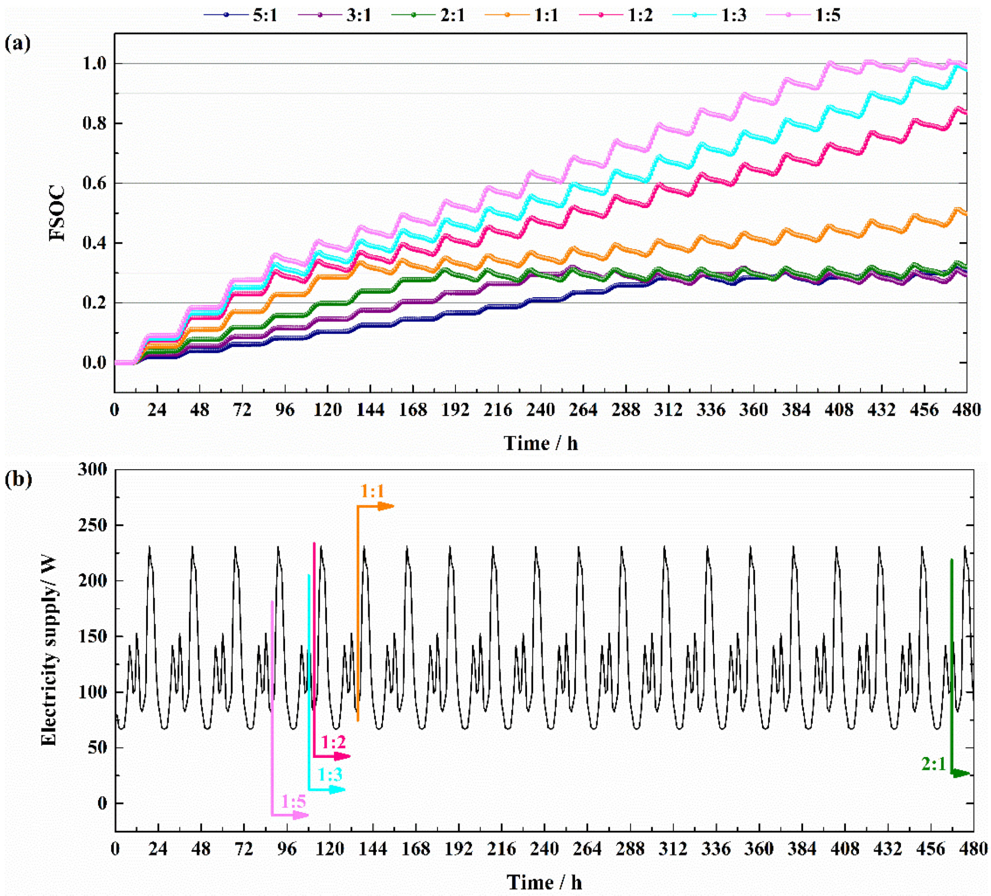

Figure 14. Hourly characteristics of the hybrid system in Andir: (**a**) FSOC of the first twenty days; (**b**) the start time of electricity supply continuity with different installed capacity ratios of WT and PV.

3.3. Summary

Taking the power supply guarantee rate and the electricity supply continuity as indicators, the standalone hybrid WT/PV system with different solar and wind resources in 26 regions of China are simulated. The recommended installed capacity ratios of the WT and PV are shown in Table 8. It can be seen that the recommended installed capacity ratio of the WT and PV is 5:1 when the total solar irradiation is less than 5040 MJ/(m^2·a) and the annual average wind velocity is in the range of 3.0~3.5 m/s. In addition, when the WER is still in this range, the scope of the recommended installed capacity ratio of the WT and PV increases with the increase of the SER. This is because when the WER is in the range of the first category, the WT dominates in the hybrid system. With the improvement of the SER, the PV plays an increasingly apparent role but does not exceed the WT. However, when the WER is in the range of the second and third categories, the PV plays an increasingly significant role in the hybrid system and exceeds the WT if the total solar irradiation is greater than 6300 MJ/(m^2·a). When the WER is scarce, the PV dominates in the hybrid system. It is worth noting that when there are several options for the installed capacity ratio of the WT and PV, the capacity with less PV should be selected because the reduction of the PV capacity could reduce the total capital cost [8,20]. In particular, the standalone hybrid WT/PV system is not recommended if the total solar irradiation is less than 5040 MJ/(m^2·a) and the annual average wind velocity is less than 2.0 m/s. Taking Chengdu as an example, although the power supply guarantee rate reaches its maximum 95.99% when the installed capacity ratios of the WT and the PV is 1:5, the continuity of the electricity supply cannot be guaranteed under any ratio.

Table 8. Recommended installed capacity ratios of WT and PV for the hybrid system with different solar and wind energy resources.

SER WER	IV <5040 MJ/(m^2·a)	III 5040~6300 MJ/(m^2·a)	II 6300~6660 MJ/(m^2·a)	I >6660 MJ/(m^2·a)
I 3.0~3.5 m/s	5:1	5:1/3:1	5:1/3:1/2:1	5:1/3:1/2:1/1:1
II 2.5~3.0 m/s	3:1/2:1	1:1	1:1/1:2	1:2
III 2.0~2.5 m/s	3:1/2:1	1:1	1:2	1:3
IV <2.0 m/s		1:2/1:3	1:3	1:5

4. Conclusions

In this paper, a standalone hybrid WT/PV system is designed for the purpose of providing electricity in rural areas. The system is simulated by the TRNSYS solver, and the input parameters are the meteorological data of the selected locations and the specifications of the WT and PV. The installed capacity ratio of the PV and WT is taken as the index of the distribution strategy to optimize the hybrid system. To obtain the optimal distribution strategies suitable for different natural resources, 26 regions of China are taken as samples. Several references for the optimal distribution strategies of the standalone hybrid WT/PV system within different natural resources are as follows:

(1) When the annual average wind velocity is in the range of 3.0~3.5 m/s, the recommended installed capacity ratios of the WT and PV are 5:1 for when the total solar irradiation is less than 5040 MJ/(m^2·a), 5:1~3:1 for when the total solar irradiation is in the range of 5040~6300 MJ/(m^2·a), 5:1~2:1 for when the total solar irradiation is in the range of 6300~6660 MJ/(m^2·a), and 5:1~1:1 for when the total solar irradiation is greater than 6300 MJ/(m^2·a).

(2) When the annual average wind velocity is in the range of 2.5~3.0 m/s, the recommended installed capacity ratios of the WT and PV are 3:1~2:1 for when the total solar irradiation is less than 5040 MJ/(m^2·a), 1:1 for when the total solar irradiation is in the range of 5040~6300 MJ/(m^2·a), 1:1~1:2 for when the total solar irradiation is in the range of 6300~6660 MJ/(m^2·a), and 1:2 for when the total solar irradiation is greater than 6300 MJ/(m^2·a).

(3) When the annual average wind velocity is in the range of 2.0~2.5 m/s, the recommended installed capacity ratios of the WT and PV are 3:1~2:1 for when the total solar irradiation is less than 5040 MJ/(m^2·a), 1:1 for when the total solar irradiation is in the range of 5040~6300 MJ/(m^2·a), 1:2 for when the total solar irradiation is in the range of 6300~6660 MJ/(m^2·a), and 1:3 for when the total solar irradiation is greater than 6300 MJ/(m^2·a).

(4) When the annual average wind velocity is less than 2.0 m/s, the recommended installed capacity ratios of the WT and PV are 1:2~1:3 for when the total solar irradiation is in the range of 5040~6300 MJ/(m^2·a), 1:3 for when the total solar irradiation is in the range of 6300~6660 MJ/(m^2·a), and 1:5 for when the total solar irradiation is greater than 6300 MJ/(m^2·a).

(5) If the total solar irradiation is less than 5040 MJ/(m^2·a) and the annual average wind velocity is less than 2.0 m/s, it is not recommended to use the standalone hybrid system because it cannot meet the power demand.

Author Contributions: Y.Y.: conceptualization, data curation, funding acquisition, writing—original draft. Q.W.: writing—review and editing. S.L.: investigation, methodology. L.Z.: software, visualization. All authors have read and agreed to the published version of the manuscript.

Funding: This research and the APC was funded by Science and Technology Innovation Plan of Shanghai Science and Technology Commission: Shanghai Sailing Program grant number 21YF1430500.

Institutional Review Board Statement: Not applicable.

Informed Consent Statement: Not applicable.

Conflicts of Interest: The authors declare that they have no known competing financial interests or personal relationships that could have appeared to influence the work reported in this paper.

Abbreviations

WT	Wind turbine
PV	Photovoltaic panel
TRNSYS	Transient system simulator
DC	Direct current
AC	Alternating current
NOCT	Nominal operating cell temperature
FSOC	Fractional state of charge
SER	Solar energy resources
WER	Wind energy resources

References

1. Weschenfelder, F.; Leite, G.D.P.; da Costa, A.C.A.; Vilela, O.D.; Ribeiro, C.M.; Ochoa, A.A.V.; Araujo, A.M. A review on the complementarity between grid-connected solar and wind power systems. *J. Clean Prod.* **2020**, *257*, 10. [CrossRef]
2. Lehtola, T.; Zahedi, A. Solar energy and wind power supply supported by storage technology: A review. *Sustain. Energy Technol. Assess.* **2019**, *35*, 25–31. [CrossRef]
3. Fant, C.; Adam Schlosser, C.; Strzepek, K. The impact of climate change on wind and solar resources in southern Africa. *Appl. Energy* **2016**, *161*, 556–564. [CrossRef]
4. Sun, W.; Harrison, G.P. Wind-solar complementarity and effective use of distribution network capacity. *Appl. Energy* **2019**, *247*, 89–101. [CrossRef]
5. Carvalho, D.B.; Guardia, E.C.; Marangon Lima, J.W. Technical-economic analysis of the insertion of PV power into a wind-solar hybrid system. *Sol. Energy* **2019**, *191*, 530–539. [CrossRef]
6. Buonomano, A.; Calise, F.; d'Accadia, M.D.; Vicidomini, M. A hybrid renewable system based on wind and solar energy coupled with an electrical storage: Dynamic simulation and economic assessment. *Energy* **2018**, *155*, 174–189. [CrossRef]
7. Alturki, F.; Al-Shamma'a, A.; Farh, H.M.H.; Alsharabi, K. Optimal sizing of autonomous hybrid energy system using supply-demand-based optimization algorithm. *Int. J. Energy Res.* **2020**, *45*, 605–625. [CrossRef]
8. Al-Ghussain, L.; Ahmed, H.; Haneef, F. Optimization of hybrid PV-wind system: Case study Al-Tafilah cement factory, Jordan. *Sustain. Energy Technol. Assess.* **2018**, *30*, 24–36. [CrossRef]
9. Li, C.; Ge, X.; Zheng, Y.; Xu, C.; Ren, Y.; Song, C.; Yang, C. Techno-economic feasibility study of autonomous hybrid wind/PV/battery power system for a household in Urumqi, China. *Energy* **2013**, *55*, 263–272. [CrossRef]
10. Yang, H.; Zhou, W.; Lu, L.; Fang, Z. Optimal sizing method for stand-alone hybrid solar–wind system with LPSP technology by using genetic algorithm. *Sol. Energy* **2008**, *82*, 354–367. [CrossRef]
11. Yang, H.X.; Zhou, W.; Lou, C.Z. Optimal design and techno-economic analysis of a hybrid solar-wind power generation system. *Appl. Energy* **2009**, *86*, 163–169. [CrossRef]
12. Ekren, O.; Ekren, B.Y.; Ozerdem, B. Break-even analysis and size optimization of a PV/wind hybrid energy conversion system with battery storage—A case study. *Applied Energy* **2009**, *86*, 1043–1054. [CrossRef]
13. Dihrab, S.S.; Sopian, K. Electricity generation of hybrid PV/wind systems in Iraq. *Renew. Energy* **2010**, *35*, 1303–1307. [CrossRef]
14. Shivam, K.; Tzou, J.-C.; Wu, S.-C. Multi-Objective Sizing Optimization of a Grid-Connected Solar–Wind Hybrid System Using Climate Classification: A Case Study of Four Locations in Southern Taiwan. *Energies* **2020**, *13*, 2505. [CrossRef]
15. Al-Karaghouli, A.; Kazmerski, L.L. Optimization and life-cycle cost of health clinic PV system for a rural area in southern Iraq using HOMER software. *Sol. Energy* **2010**, *84*, 710–714. [CrossRef]
16. Khan, M.J.; Iqbal, M.T. Pre-feasibility study of stand-alone hybrid energy systems for applications in Newfoundland. *Renew. Energy* **2005**, *30*, 835–854. [CrossRef]
17. Zandi, M.; Bahrami, M.; Eslami, S.; Gavagsaz-Ghoachani, R.; Payman, A.; Phattanasak, M.; Nahid-Mobarakeh, B.; Pierfederici, S. Evaluation and comparison of economic policies to increase distributed generation capacity in the Iranian household consumption sector using photovoltaic systems and RETScreen software. *Renew. Energy* **2017**, *107*, 215–222. [CrossRef]
18. Owolabi, A.B.; Nsafon, B.E.K.; Roh, J.W.; Suh, D.; Huh, J.-S. Validating the techno-economic and environmental sustainability of solar PV technology in Nigeria using RETScreen Experts to assess its viability. *Sustain. Energy Technol. Assess.* **2019**, *36*, 100542. [CrossRef]

19. Bakić, V.; Pezo, M.; Stevanović, Ž.; Živković, M.; Grubor, B. Dynamical simulation of PV/Wind hybrid energy conversion system. *Energy* **2012**, *45*, 324–328. [CrossRef]
20. Panayiotou, G.; Kalogirou, S.; Tassou, S. Design and simulation of a PV and a PV–Wind standalone energy system to power a household application. *Renew. Energy* **2012**, *37*, 355–363. [CrossRef]
21. Zappa, W.; van den Broek, M. Analysing the potential of integrating wind and solar power in Europe using spatial optimisation under various scenarios. *Renew. Sustain. Energy Rev.* **2018**, *94*, 1192–1216. [CrossRef]
22. Nguyen, H.T.; Safder, U.; Nguyen, X.Q.N.; Yoo, C. Multi-objective decision-making and optimal sizing of a hybrid renewable energy system to meet the dynamic energy demands of a wastewater treatment plant. *Energy* **2020**, *191*, 18. [CrossRef]
23. Sinha, S.; Chandel, S.S. Review of software tools for hybrid renewable energy systems. *Renew. Sustain. Energy Rev.* **2014**, *32*, 192–205. [CrossRef]
24. Mazzeo, D.; Baglivo, C.; Matera, N.; Congedo, P.M.; Oliveti, G. A novel energy-economic-environmental multi-criteria decision-making in the optimization of a hybrid renewable system. *Sust. Cities Soc.* **2020**, *52*, 101780. [CrossRef]
25. Meng, S.; Sun, R.; Guo, F. Does the use of renewable energy increase carbon productivity?—An empirical analysis based on data from 30 provinces in China. *J. Clean Prod.* **2022**, *365*, 132647. [CrossRef]
26. Zhou, N.; Price, L.; Yande, D.; Creyts, J.; Khanna, N.; Fridley, D.; Lu, H.; Feng, W.; Liu, X.; Hasanbeigi, A.; et al. A roadmap for China to peak carbon dioxide emissions and achieve a 20% share of non-fossil fuels in primary energy by 2030. *Appl. Energy* **2019**, *239*, 793–819. [CrossRef]
27. Energy Research Institute of National Development and Reform Commission. *China 2050 High Renewable Energy Penetration Scenario and Roadmap Study*; Energy Research Institute of National Development and Reform Commission: Beijing, China, 2015.
28. Liu, L.; Wang, Z.; Wang, Y.; Wang, J.; Chang, R.; He, G.; Tang, W.; Gao, Z.; Li, J.; Liu, C.; et al. Optimizing wind/solar combinations at finer scales to mitigate renewable energy variability in China. *Renew. Sustain. Energy Rev.* **2020**, *132*, 110151. [CrossRef]
29. He, C.; Liu, J.; Xu, F.; Zhang, T.; Chen, S.; Sun, Z.; Zheng, W.; Wang, R.; He, L.; Feng, H.; et al. Improving solar radiation estimation in China based on regional optimal combination of meteorological factors with machine learning methods. *Energy Convers. Manag.* **2020**, *220*, 113111. [CrossRef]
30. Ren, G.; Wan, J.; Liu, J.; Yu, D. Characterization of wind resource in China from a new perspective. *Energy* **2019**, *167*, 994–1010. [CrossRef]
31. Feng, Y.; Que, L.; Feng, J. Spatiotemporal characteristics of wind energy resources from 1960 to 2016 over China. *Atmos. Ocean. Sci. Lett.* **2020**, *13*, 136–145. [CrossRef]
32. He, G.; Kammen, D.M. Where, when and how much solar is available? A provincial-scale solar resource assessment for China. *Renew. Energy* **2016**, *85*, 74–82. [CrossRef]
33. Fry, B. Simulation of Grid-Tied Building Integrated Photovoltaic Systems. Master's Thesis, Solar Energy Laboratory, University of Wisconsin, Madison, WI, USA, 1999.
34. White, F. *Fluid Mechanics*, 3rd ed.; Mc Graw Hill: New York, NY, USA, 1994.
35. Putnam, P.C.; Gerald, W.K. *Putnam's Power from the Wind*, 2nd ed.; Van Nostrand Reinhold Company: New York, NY, USA, 1982.
36. Guangzhou Infinite Windpower Generator Manufacture Co., Ltd. Available online: http://23395.china-nengyuan.com/ (accessed on 1 July 2022).
37. Kebede, A.A.; Coosemans, T.; Messagie, M.; Jemal, T.; Behabtu, H.A.; Van Mierlo, J.; Berecibar, M. Techno-economic analysis of lithium-ion and lead-acid batteries in stationary energy storage application. *J. Energy Storage* **2021**, *40*, 102748. [CrossRef]
38. Chen, H.; Cong, T.N.; Yang, W.; Tan, C.; Li, Y.; Ding, Y. Progress in electrical energy storage system: A critical review. *Prog. Nat. Sci.* **2009**, *19*, 291–312. [CrossRef]
39. Cabello, G.M.; Navas, S.J.; Vázquez, I.M.; Iranzo, A.; Pino, F.J. Renewable medium-small projects in Spain: Past and present of microgrid development. *Renew. Sustain. Energy Rev.* **2022**, *165*, 112622. [CrossRef]
40. Das, B.K.; Hoque, N.; Mandal, S.; Pal, T.K.; Raihan, M.A. A techno-economic feasibility of a stand-alone hybrid power generation for remote area application in Bangladesh. *Energy* **2017**, *134*, 775–788. [CrossRef]
41. Yuan, P.; Duanmu, L.; Wang, Z.; Li, X.; Shu, H. Analysis of law of domestic electricity consumption for rural residences at some town in Chifeng under various temporal scales. *J. Dalian Univ. Technol.* **2020**, *60*, 165–173.
42. Qiu, H.G.; Yan, J.B.; Li, D.W.; Han, W. Residential energy consumption in rural China: Current situation and determinants for future trend—An empirical study based on filed survey data of 4 provinces. *China Soft Sci.* **2015**, *11*, 28–38.